Nonlinear Analysis: Real World Applications 13 (2012) 2794–2803

Contents lists available at SciVerse ScienceDirect

Nonlinear Analysis: Real World Applications

journal homepage: www.elsevier.com/locate/nonrwa

Velocity of pulses in discrete excitable systems

J.I. Arana, L.L. Bonilla *

G. Millán Institute of Fluid Dynamics, Nanoscience and Industrial Mathematics, Universidad Carlos III de Madrid, Avenida de la Universidad 30, 28911 Leganés, Spain

ARTICLE INFO

Article history:
Received 14 November 2011
Accepted 15 March 2012

Keywords:
Excitable systems
Nonlinear pulses and wave fronts
Discrete FitzHugh–Nagumo system
Matched asymptotic expansions

ABSTRACT

The pulse solution of the spatially discrete excitable FitzHugh–Nagumo (FHN) system is approximately constructed using matched asymptotic expansions in the limit of large time scale separation (as measured by a small dimensionless parameter ϵ). The pulse profile typically consists of slowly varying regions of the excitatory variable separated by sharp wave fronts. In the FHN system, the velocity of a pulse is decided by the interaction between its leading and trailing fronts, but the leading order approximation gives only a fair result when compared with direct numerical solutions. A higher order approximation to the wave fronts comprising the FHN pulse is found. Our approximation provides an ϵ-dependent pulse velocity that approximates much better the velocity obtained from numerical solutions. As a result, the reconstruction of the FHN pulse using the improved wave fronts is much closer to the numerically obtained pulse.

1. Introduction

Many physical and biological systems made up of smaller interacting components such as atoms, quantum wells, cells, etc. can be often described by spatially discrete nonlinear equations. They are differential–difference equations (DDEs) whose continuum limits are partial differential equations (PDEs). Examples include the motion of dislocations and their pinning due to the crystalline lattice [1,2], crystal growth and interface motion in crystalline materials [3], the pinning and motion of domain walls in semiconductor superlattices [4–7], sliding of charge density waves [8], and pulse propagation through myelinated nerves [9–11].

In spatially extended continuum media described by PDEs, traveling waves are functions of a moving coordinate and therefore they can be found by solving the associated dynamical system in the moving coordinate. Nonlinear DDEs can also have traveling waves among their solutions: these waves are easy to find numerically by comparing the time evolution of neighboring cells but proofs of their existence do not abound [12–14]. The most significant difference between nonlinear DDEs and their limiting PDEs is that the discrete systems usually have coupling thresholds for propagation of wave fronts. For instance, a bistable parabolic PDE with a cubic source term typically has wave front solutions moving with a diffusion dependent velocity. The equation

$$\partial_t u = D\,\partial_x^2 u + g(u), \quad -\infty < x < \infty, \tag{1}$$

$$g(u) = u(u-a)(2-u), \tag{2}$$

with $0 < a < 2$ such that $\int_0^2 g(u)\,du < 0$, has a wave front solution $u(x,t) = U(x-ct)$ moving with positive velocity $c > 0$ and boundary conditions $U(\pm\infty) = 1 \pm 1$ [15]. The DDE obtained by substituting centered finite differences instead of derivatives in the PDE (1),

$$\dot{u}_n = d\,(u_{n+1} + u_{n-1} - 2u_n) + g(u_n), \tag{3}$$

* Corresponding author.
E-mail address: bonilla@ing.uc3m.es (L.L. Bonilla).

1468-1218/$ – see front matter
doi:10.1016/j.nonrwa.2012.03.016

where $\dot{u} = du/dt$, has traveling wave front solutions only if the diffusion d (which measures coupling between neighboring cells) is larger than a certain positive threshold value. For smaller diffusion, the corresponding stable solution is a stationary wave front and we say that the wave front is pinned. If we vary the parameter a, Eq. (1) has wave front solutions with zero velocity for the single value $a = 1$, such that $\int_0^2 g(u)\,du = 0$, and the wave fronts move with positive (resp. negative) speed if $a > 1$ (resp. $a < 1$) [15]. In contrast with this simple behavior, Eq. (3) has wave front solutions that move with non-zero speed for $a < a_{cl}(d)$ and $a > a_{cr}(d)$ (see Fig. 1.2(a) of [16] and Chapter 4 of [6]). In the continuum limit, $\epsilon \to 0$, $d = D/\epsilon^2$, the width of the pinning interval given by $a_{cr} - a_{cl}$ tends exponentially fast to zero. Mathematical understanding of the propagation failure of wave fronts in DDE was much advanced by Keener's use of comparison principles to characterize the pinning and motion of wave fronts for spatially discrete reaction–diffusion equations such as Eq. (1) [17]. See also [18,19].

As could have been expected, DDE systems exhibit a greater variety of waves and dynamical behavior than scalar DDEs. As in the case of continuous extended excitable systems [20,11], excitable systems described by DDE systems display pulses and wave trains among their solutions. For the spatially discrete FitzHugh–Nagumo (FHN) system, pulses and wave trains are asymptotically constructed in [16] and in [21], respectively. Rigorous proofs of the existence of pulses for the discrete FHN system can be found in [22] and a proof of their nonlinear stability in [23]. A more general discrete excitable system with Hodgkin–Huxley dynamics that describes propagation along myelinated nerves is studied in [24]. A discrete excitable FHN system in which both variables have discrete diffusivities may give rise to stationary patterns that depend on the initial conditions and be used to store images in two-dimensional space [25]. Excitable systems on a lattice can display more complex patterns such as spiral waves [26,27]. In other cases, the discrete system of equations contains terms with time delay [28,29] or the coupling between different FHN units is delayed in time and a variety of different behaviors are possible [30]. The strategy in all constructions of traveling waves is to assume that, as in the scalar case, the solutions are waves traveling with constant velocity and then to exploit the large separation in time scales characteristic of these excitable media. The existence of different time scales allows us to separate the regions of pulses and wave trains where there are sharp variations of u_n from those regions where u_n varies smoothly. Typically the regions of sharp variations are approximated by traveling waves of a scalar DDE [16]. All these constructions of traveling waves use leading order asymptotics and yield wave velocities that are independent of the small perturbation parameter ϵ. Comparison with numerical solutions shows that there are significant differences between the predicted and numerically calculated wave speeds [16]. Thus it seems natural to correct the results of leading order asymptotics to attain better agreement.

When dealing with PDEs, rescaling the space variable is a usual ingredient of a perturbation scheme, but we cannot do this with a DDE. In this paper, we propose a general way to correct leading order constructions of traveling waves for systems of DDEs and, for the sake of simplicity, we shall present our results for the FHN system. In Section 2, we recall the leading order construction of the pulses for the FHN system [16]. The correction to the leading order result for the leading and trailing wave fronts comprising a pulse is given in Section 3. This section also includes graphs of the wave front velocity versus ϵ. The corrected descriptions of the leading and trailing fronts are used to obtain a corrected description of the FHN pulse in Section 4. Related corrections are described in [7] for a much more complex discrete model of photoexcited undoped semiconductor superlattices that contains nonlinear convective terms and algebraic constraints. Section 5 contains a comparison with the numerical solution of the FHN system and the last section states our conclusions.

2. Leading order construction of the FHN pulse

In this section, we recall the asymptotic construction of pulses for the discrete FHN system given in [16] which uses ideas similar to the construction for continuous excitable media [20]. The following nondimensional equations govern the discrete FHN system:

$$\epsilon\,\dot{u}_n = d\,(u_{n+1} - 2u_n + u_{n-1}) + g(u_n) - v_n, \tag{4}$$

$$\dot{v}_n = u_n - Bv_n, \tag{5}$$

$n = 0, \pm 1, \ldots$, $g(u) = u(u-a)(2-u)$ and $\epsilon \ll 1$. u_n and v_n are called the excitatory (or potential) and recovery variables, respectively. For $0 < B < B_1 \equiv 4/(2-a)^2$, the only uniform stationary solution is $u_n = 0 = v_n$ (critical point), whereas for $B > B_1$, there are two other critical points, one over each of the other two branches of the cubic source $g(u)$. We fix the parameters $0 < B < B_1$, $d > 0$, $a < a_{cl}(d)$ (the case $a > a_{cr}(d)$ follows by symmetry) and ϵ smaller than a certain critical value, $\epsilon_c(a, d)$, which we shall calculate approximately below. The leading order description of a pulse is as follows. A pulse consists of regions of smooth variation of u on the time scale t, separated by sharp interfaces in which u varies rapidly on the time scale t/ϵ. In the regions where u varies smoothly, we can set $\epsilon = d = 0$, thereby obtaining the reduced problem,

$$g(u_n) - v_n = 0, \tag{6}$$

$$\frac{dv_n}{dt} = u_n - B\,v_n. \tag{7}$$

These regions are separated by sharp interfaces (moving fronts) at which u_n varies rapidly as $u_n(t) = U(z)$, $v_n(t) = V(z)$, with $z = n - ct/\epsilon$. There, to leading order,

$$-c\,\frac{d\mathcal{U}}{dz} = d\,[\mathcal{U}(z+1) - 2\mathcal{U}(z) + \mathcal{U}(z-1)] + g(\mathcal{U}(z)) - \mathcal{V}(z), \tag{8}$$

$$-c\,\frac{d\mathcal{V}}{dz}=0. \tag{9}$$

Thus $\mathcal{V}$ is a constant equal to the value $v_n(t)$ at the last point in the region of smooth variation before the front. Eq. (8) is a scalar DDE having two different wave front solutions $u=\mathcal{U}(z)$. *Increasing front* (IF) solutions satisfy $d\mathcal{U}/dz>0$ and $\mathcal{U}(-\infty)=u^{(1)}(\mathcal{V})$ and $\mathcal{U}(\infty)=u^{(3)}(\mathcal{V})$, whereas *decreasing front* (DF) solutions have $d\mathcal{U}/dz<0$ and $\mathcal{U}(-\infty)=u^{(3)}(\mathcal{V})$, $\mathcal{U}(\infty)=u^{(1)}(\mathcal{V})$. Here $u^{(1)}(v)<u^{(2)}(v)<u^{(3)}(v)$ are the three zeros of $g(u)-v$ for appropriate values of v. We can now discuss different regions in the asymptotic description of a pulse.

a. The region of smooth variation of u in front of the pulse, described by Eqs. (6) and (7). In this region, $u_n=u^{(1)}(v_n)$, so that
$$\frac{dv_n}{dt}=u^{(1)}(v_n)-B\,v_n,$$
and initial data evolve exponentially fast towards equilibrium, $u_n=v_n=0$.
b. The pulse leading edge. Let $v(t)$ be the value of v_n at the last point of the region in front of the pulse. Eventually, $v\to 0$. At the leading edge, $u_n(t)=\mathcal{U}(n-ct/\epsilon)$ is a DF satisfying $\mathcal{U}(-\infty)=u^{(3)}(v)$, $U(\infty)=u^{(1)}(v)$, and moving towards the right with speed $C=c(a,d,v)/\epsilon$ measured in points per unit time t. It is convenient to call $c_-(v)=c(a,d,v)$. Eventually, $C\sim c_-(0)/\epsilon$, and u_n decreases from $u_n=2$ to $u_n=0$ across the leading edge of the pulse.
c. Region between fronts: $u_n=u^{(3)}(v_n)$ and
$$\frac{dv_n}{dt}=u^{(3)}(v_n)-B\,v_n.$$
There are finitely many points in this region. On its far right, $v_n=v\to 0$. As we move towards the left, v_n increases until it reaches a certain value $V(t)$ corresponding to that in the trailing wave front.
d. Trailing wave front: $v_n(t)=\mathcal{V}(z)=V$, and $u_n(t)=\mathcal{U}(z)$ is an IF satisfying Eq. (8) with boundary conditions $\mathcal{U}(-\infty)=u^{(1)}(V)$ and $\mathcal{U}(\infty)=u^{(3)}(V)$. This front increases monotonically with z and it moves with speed $C=c(a,d,w)/\epsilon$ measured in points per unit time t. It is convenient to denote $c_+(V)=c(a,d,V)$. We shall indicate how to determine V below. Clearly, if the pulse is to move rigidly, we should have $c_+(V)=c_-(0)$ after a sufficiently long transient period.
e. Pulse tail. Again $u_n=u^{(1)}(v_n)$ and $dv_n/dt=u^{(1)}(v_n)-Bv_n$. Sufficiently far to the left, $v_n=u_n=0$.

The number of points between wave fronts of the pulse is not arbitrary. Let τ be the delay between fronts, i.e. the time elapsed from the instant at which the leading front traverses the point $n=N$ to the instant when the trailing front is at $n=N$. Clearly,

$$\tau=\int_{v(t-\tau)}^{V(t)}\frac{dv}{u^{(3)}(v)-Bv}. \tag{10}$$

The number of points between fronts, $l(t)$, can be calculated as

$$l=\frac{1}{\epsilon}\int_{t-\tau}^{t}c_-(v(t))\,dt. \tag{11}$$

On the other hand, the separation between fronts satisfies the equation

$$\frac{dl}{dt}=\frac{c_-(v(t))-c_+(V(t))}{\epsilon}. \tag{12}$$

The three Eqs. (10)–(12) can be solved to obtain the three unknowns τ, l and $V(t)$. (The function $v(t)$ is determined by solving Eq. (7) with $u_n=u^{(1)}(v_n)$ in the region to the left of the leading front).

After a transient period, $v(t)\to 0$ and $V(t)\to V$ (a constant value), so that we have the simpler expressions

$$\tau=\int_0^V\frac{dv}{u^{(3)}(v)-Bv}, \tag{13}$$

$$\frac{dl}{dt}=\frac{c_-(0)-c_+(V)}{\epsilon}, \tag{14}$$

instead of Eqs. (10) and (12), respectively. The number of points at the pulse top is now

$$l=\frac{c_-(0)\tau}{\epsilon}=\frac{c_-(0)}{\epsilon}\int_0^V\frac{dv}{u^{(3)}(v)-Bv}. \tag{15}$$

This equation yields V as a function of l. Then, Eq. (14) becomes an autonomous differential equation for l that has a stable constant solution at $l=l^*$ such that $c_-(0)=c_+(V(l))$. At $l=l^*$, the right hand side of Eq. (14) has a slope $-[u^{(3)}(V)-BV]\,c_+'(V)/c_-(0)<0$.

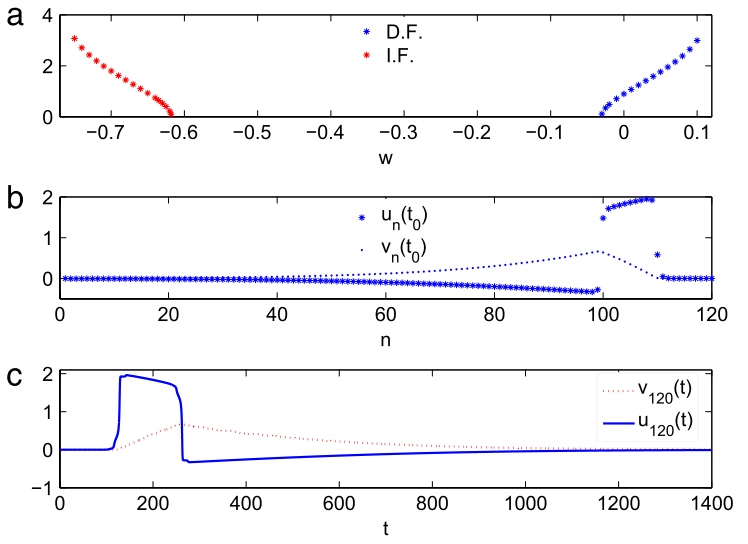

Fig. 1. (a) Numerically obtained wave front velocity for Eq. (1) with $g(u) = u(u-a)(2-u) - w$, $d = 0.1$ and $a = B = 0.5$. The horizontal line graphically yields V^* such that $c_+(V^*) = c_-(0)$. (b) Profiles of the FHN pulse for $\epsilon = 0.003$. (c) Trajectories of one point, $u_{120}(t)$, $v_{120}(t)$, as the FHN pulse traverses it.

Recapitulating, for appropriate initial conditions, leading and trailing fronts of a pulse evolve until l reaches its stable value at which $c_-(0) = c_+(V(l^*))$ and Eq. (15) holds. To compute l^*, we first determine $V^* = V(l^*)$ by using $c_-(0) = c_+(V(l^*))$. Then, we calculate $\tau = \tau^*$ (which does not depend on ϵ!) from Eq. (13) and $l^* = c_-(0)\tau^*/\epsilon$. Our construction breaks down if the number of points between fronts falls below 1. This yields an upper bound for the critical value of ϵ above which pulse propagation fails: $\epsilon_c \sim c_-(0)\tau^*$.

The asymptotic length of the pulse tail is obtained by first calculating the time needed for v_n to go from a neighborhood of the fixed point 0 to $V(l^*)$ to the left of the trailing front:

$$t = \int_v^V \frac{dv}{Bv - u^{(1)}(v)} \sim \int_0^V \left[\frac{1}{Bv - u^{(1)}(v)} - \frac{1}{[B - u^{(1)'}(0)]v}\right] dv + \frac{\ln(V/v)}{B - u^{(1)'}(0)},$$

with $u^{(1)'}(0) = 1/g'(0) < 0$, and therefore

$$v(t) \sim V \exp\left[-\left(B - \frac{1}{g'(0)}\right)(t - T_1)\right], \tag{16}$$

$$T_1 = \int_0^V \left[\frac{1}{Bv - u^{(1)}(v)} - \frac{g'(0)}{[Bg'(0) - 1]v}\right] dv, \tag{17}$$

for long times such that $v(t)$ is sufficiently close to 0. The time needed for $v(t)$ to go from V to V/e is then $T = T_1 + |g'(0)|/[1 - Bg'(0)]$. The tail length is then $L = c_-(0)T/\epsilon$.

Fig. 1 illustrates our construction. Setting $w = 0$, we find a velocity $c_-(0)$ of the DF. Then, a horizontal line that intersects $c_-(w)$ at $w = 0$, as shown in Fig. 1(a), yields $c_+(w) = c_-(0)$ at $w = V^*$. Eq. (13) produces the pulse duration τ^* and Eq. (14) gives the pulse width l^* between its two fronts. The FHN pulse profile is shown in Fig. 1(b) and the trajectory of a single point traversed by the pulse is depicted in Fig. 1(c).

3. $O(\epsilon)$ construction of the wave fronts comprising a pulse

3.1. Exact formula for the wave front profile

To correct the previous asymptotic theory of pulses, we need to improve the description of wave fronts. To this end, we use the fact that DF or IF profiles are monotonic functions of a variable $z = n - ct/\epsilon$, where c is the front velocity and we consider fronts moving from left to right ($c > 0$). Thus

$$u_n(t) = \mathcal{U}(z), \qquad v_n(t) = \mathcal{V}(z), \tag{18}$$

with $\mathcal{U}'(z) > 0$ (resp. <0) for IF (resp. DF). In either case, we can find

$$z = Z(U) \quad \text{which solves} \quad \mathcal{U}(z) = U. \tag{19}$$

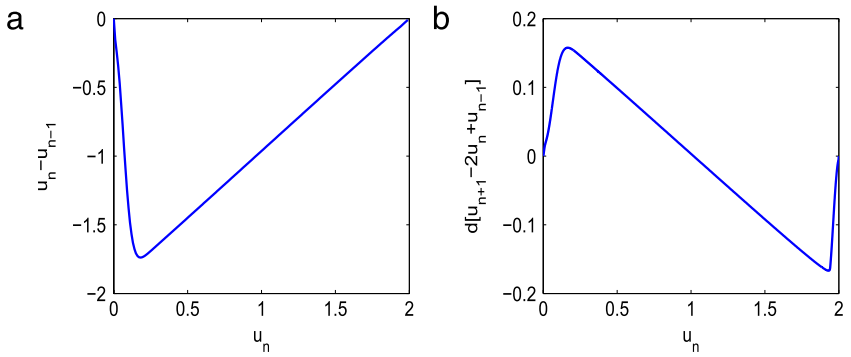

Fig. 2. (a) Backward and forward differences as functions of u_n for a leading order DF at constant $v = 0$ in the interval (v_-, v_+). (b) Second order centered difference as a function of u_n for the same front. Parameter values as in Fig. 1.

Therefore, the finite differences

$$D^{\mp}u_n \equiv \pm[u_n - u_{n\mp1}] = \pm[\mathcal{U}(z) - \mathcal{U}(z \mp 1)] = \pm[u_n - \mathcal{U}(Z(u_n) \mp 1)],$$
$$D^{+}D^{-}u_n = u_{n+1} + u_{n-1} - 2u_n = \mathcal{U}(Z(u_n) + 1) + \mathcal{U}(Z(u_n) - 1) - 2u_n,$$

can be considered to be functions of u_n. To leading order as $\epsilon \to 0$, $\mathcal{U}(z) \sim \mathcal{U}^{(0)}(n - c^{(0)}t/\epsilon)$, $\mathcal{V}(z) = v$, as explained in the previous section. For a DF calculated with the leading order theory of Section 2, Fig. 2(a) and (b) show the differences $D^{\pm}u_n$ and $D^{+}D^{-}u_n$ as functions of u_n. Note that these differences vanish for u_n on the nullcline $v = g(u_n)$.

Since the second difference $D^{+}D^{-}u_n$ is a function of u_n, we can derive from the equation for $v_n = \mathcal{V}(z)$:

$$-c\frac{dv_n}{dz} = \epsilon(u_n - Bv_n), \tag{20}$$

and from the equation for the wave front profile, $u_n = \mathcal{U}(z)$,

$$-c\frac{du_n}{dz} = d\,D^{+}D^{-}u_n + g(u_n) - v_n, \tag{21}$$

the following *exact* equation for v_n as a function of u_n:

$$\frac{dv_n}{du_n} = \epsilon\,\frac{u_n - Bv_n}{g(u_n) - v_n + d\,(D^{+}D^{-}u_n)(u_n)}. \tag{22}$$

3.2. Corrected decreasing front (leading front of a pulse)

Now we integrate this equation and iterate the result starting from the value $v_n(u_\infty) = v$ (corresponding to $t \to -\infty$ because $u_n(t) = \mathcal{U}(z)$, $z = n - ct/\epsilon$), thereby obtaining

$$v_n \sim v + \epsilon\int_{u_\infty}^{u_n}\frac{(u - B\,v)\,du}{g(u) - v + d\,\mathcal{D}^{(0)}(u)}, \tag{23}$$

up to terms of order ϵ^2. In Eq. (23), the leading order approximation to the second difference $(D^{+}D^{-}u_n)(u_n)$ has been denoted by $\mathcal{D}^{(0)}(u_n)$; cf. Fig. 2(b).

The starting point u_∞ is on the nullcline $v = g(u)$, and therefore it satisfies $g(u_\infty) = v$. This creates problems of convergence for the integral in Eq. (23) because the boundary condition $\mathcal{U}(\infty) = u_\infty$ seems to imply that the finite differences on this tail of the wave front are zero and therefore that the denominator in Eq. (23) would vanish. We find a similar problem as $n \to -\infty$ and the final point of the wave front approaches the other nullcline. An easy way out is the case in which $v = v_*$ corresponds exactly to a uniform stationary solution (critical point). Then, $u_\infty = u_*$, the value corresponding to the same critical point, the integrand in Eq. (23) has a finite limit as $u_n \to u_\infty$ and the integral converges. For $0 < B < B_1$, the only critical point is $u_* = v_* = 0$, so that we would have $u_\infty = 0$ for $v = 0$. For $B > B_1$, we have two other possible critical points. If $v \neq v^*$, then we need to make sure that $\mathcal{D}^{(0)}(u_{-\infty}) \neq 0$ to avoid having a singular integrand at $u = u_\infty$. How can we achieve this?

Consider the case of only one critical point ($0 < B < B_1$). The leading front of a pulse is a decreasing front (DF) starting at the critical point $u_* = v_* = 0$ and ending on the third branch of the nullcline $v = g(u)$, whereas the trailing front is an increasing front (IF) that should join non-critical points on the first and third branches of the nullcline $v = g(u)$.

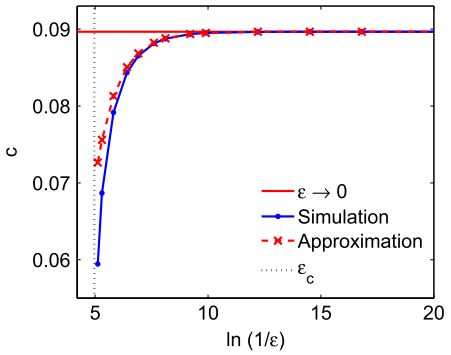

Fig. 3. Velocity of the DF as a function of $-\ln\epsilon$ for a DF with $v_{-\infty}=0$.

For the DF, the integrand of Eq. (23) is not singular at the critical point $u_\infty = 0$ and the corrected wave front is the solution of the fast Eq. (21),

$$-c\,\frac{d\mathcal{U}}{dz}+v_n(\mathcal{U})-g(\mathcal{U})-d\,(D^+D^-u_n)(\mathcal{U})=0 \tag{24}$$

or, equivalently, the time-dependent version of this equation:

$$\frac{du_n}{dt}=d\,(u_{n+1}-2u_n+u_{n-1})+g(u_n)-v_n(u_n),\qquad T=\epsilon\,(t-t_0) \tag{25}$$

($t_0=0$ for the DF and $t_0=t_v$ for the IF explained below), with the boundary conditions

$$u_n(-\infty)=\mathcal{U}(+\infty)=0,\qquad u_n(+\infty)=\mathcal{U}(-\infty)=u^{(3)}(v'),\quad v'>0. \tag{26}$$

In this expression, the value $v'>0$ is determined by solving Eqs. (23) and (24) until the first branch of $g(u)$ is reached. The velocity of the DF is now a function of ϵ and Fig. 3 shows that it is a much better approximation of the numerically calculated front velocity than that given by the leading order theory.

3.3. Corrected increasing front (trailing front of a pulse)

The case of the IF is more complicated: the integrand of Eq. (23) is now singular when $u_{+\infty}$ is on the third branch of the nullcline $v=g(u)$. To solve this problem, we first calculate the $O(\epsilon)$ correction to the slow scale Eq. (6) when u_n is on the third branch of the nullcline $v=g(u)$. The leading order approximation during the slow scale is $u_n=\Phi(v_n)$ ($\Phi(v_n)=u^{(3)}(v_n)$ for our IF). Inserting this function in Eq. (7), we get

$$\frac{dv_n}{dt}=\Phi(v_n)-Bv_n. \tag{27}$$

The $O(\epsilon)$ correction to the slow stage equations is obtained assuming that the discrete diffusivity is of order ϵ: $d(u_{n+1}+u_{n-1}-2u_n)=\epsilon d'\mathcal{D}^{(0)}(u_n)$. Then we find $u_n(t;\epsilon)\sim u_n+\epsilon u_n^{(1)}$, $v_n(t;\epsilon)\sim v_n+\epsilon v_n^{(1)}$, with

$$\frac{dv_n^{(1)}}{dt}+Bv_n-u_n^{(1)}=0, \tag{28}$$

$$g'(\Phi(v_n))u_n^{(1)}-v_n^{(1)}=\frac{\Phi(v_n)-Bv_n}{g'(\Phi(v_n))}-d'\mathcal{D}^{(0)}\Phi(v_n), \tag{29}$$

where $\Phi(v)=u^{(3)}(v)$ on the third branch of the nullcline $v=g(u)$. Let $t=t_v$ be the time at which the zeroth order approximation (on the slow scale), $v_n(t_v)$, reaches the value v from which the zeroth order approximation to the IF would start on the fast scale: $u^{(3)}(v)$. We choose $v'=v_n(t_v-1/c)<v$ and $u_{+\infty}=u^{(3)}(v')$. We now calculate U_r^v such that the zeroth-order discrete diffusion operator at U_r^v equals the discrete diffusion operator applied to the corrected $u_n(t;\epsilon)$:

$$\mathcal{D}^{(0)}(U_r^v)=u_{n+1}(t_v;\epsilon)+u_{n-1}(t_v;\epsilon)-2u_n(t_v;\epsilon). \tag{30}$$

Similarly, another value U_l^v is calculated in the same way as U_r^v except that we use the equations for the slow stage on the first branch of the nullcline $v=g(u)$ for which $t>t_v$. These $U_{r,l}^v$ values are in $[U_l,U_r]$ such that $\mathcal{D}^{(0)}(U_{l,r})=0$. For a fixed $u\in[u_n(t_v;\epsilon),u_n(t_v-1/c;\epsilon)]$, we find another time t_u such that $u_n(t_u;\epsilon)=u$. Then, we define the first-order discrete diffusion operator by $\mathcal{D}^{(1)}(u)\equiv u_{n+1}(t_u;\epsilon)+u_{n-1}(t_u;\epsilon)-2u_n(t_u;\epsilon)$. For each $u\in[u_n(t_v;\epsilon),u_n(t_v-1/c;\epsilon)]$, we associate $\mathcal{U}$ such that

$$\mathcal{D}^{(1)}(u)=\mathcal{D}^{(0)}(\mathcal{U}). \tag{31}$$

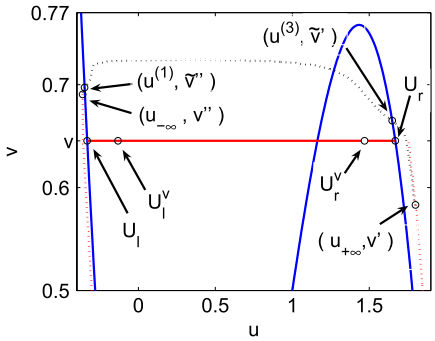

Fig. 4. Sketch of the IF construction. The nullclines are represented by solid lines and the corrected values $(u_n + \epsilon u_n^{(1)}, v_n + \epsilon v_n^{(1)})$ by dashed lines. U_l and U_r are the horizontal coordinates on the outer branches of the cubic nullcline corresponding to the value v of the vertical coordinate at which the fast zeroth-order jump between nullclines occurs. At the zeroth-order, this jump occurs at a certain time t_v. On the outer nullcline of the cubic, we define $v' = v_n(t_v - 1/c) < v$ and $u_{+\infty} = u^{(3)}(v')$, whereas on the inner nullcline of the cubic, we define $v'' = v_n(t_v - 1/c) > v$ and $u_{-\infty} = u^{(1)}(v'')$. At the points $(u^{(1)}(\tilde{v}''), \tilde{v}'')$ and $(u^{(3)}(\tilde{v}'), \tilde{v}')$, the dashed lines intersect the outer branches of the cubic nullcline. Finally, U_r^v and U_l^v are defined by Eq. (30) and belong to the interval (U_l, U_r).

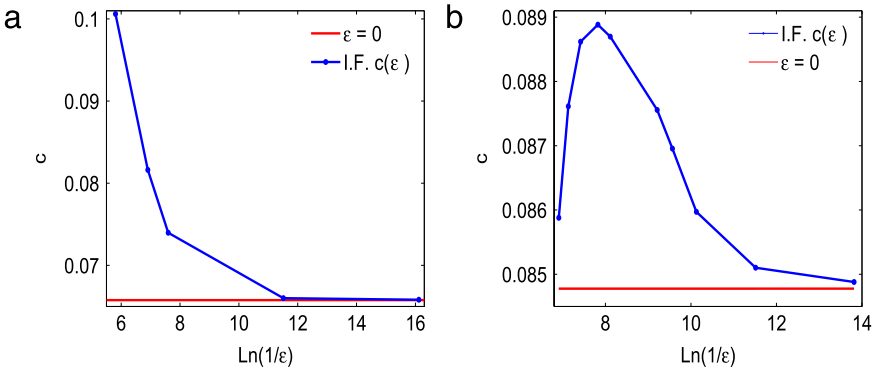

Fig. 5. Wave front velocity as a function of $-\ln\epsilon$ for an IF with fixed (a) $v_{+\infty} = v' = 0.63572$, and (b) $v = 0.63586$. For parameter values as in Fig. 1, we have marked with dots the critical value $\epsilon_c \approx 0.007$ above which no stable pulses are found.

$\mathcal{U}$ is in the interval $[U_l^v, U_r^v]$. At $t = t_v+$ (immediately after the fast stage ends), the slow stage on the first branch of $v = g(u)$ starts at $v = v'$. Fig. 4 sketches the construction of the IF and shows the values $U_{l,r}^v$, $U_{l,r}$, v', v'', $\tilde{v}'$, $\tilde{v}''$, and $u_{\pm\infty}$.

In the fast stage of the wave front connecting $(u_{+\infty}, v')$ to $(u_{-\infty}, v'')$, we use an equation similar to Eq. (23),

$$v_n \sim v' + \epsilon \int_{u_\infty}^{u_n} \frac{(u - B\,v)\,du}{g(u) - v + d\,\mathcal{D}^{(1)}(u)}, \tag{32}$$

except that we have replaced $\mathcal{D}^{(1)}(u)$ instead of $\mathcal{D}^{(0)}(u)$ and $v_n \sim v'$ at the leading order. The IF is a solution of Eqs. (24) and (32) with boundary conditions:

$$u_n(-\infty) = \mathcal{U}(+\infty) = \tilde{u}_{+\infty} \equiv u^{(3)}(\tilde{v}'), \qquad u_n(+\infty) = \mathcal{U}(-\infty) = \tilde{u}_{-\infty} \equiv u^{(1)}(\tilde{v}''), \tag{33}$$

where

$$g(\tilde{u}_{+\infty}) = \tilde{v}', \qquad g(\tilde{u}_{-\infty}) = \tilde{v}''. \tag{34}$$

The IF ends at a point $(u_{-\infty}, v'')$ on the corrected first branch of the nullcline, namely the solution of Eqs. (27)–(29) with $\Phi(v) = u^{(1)}(v)$. The velocity of the IF is a function of ϵ and Fig. 5 shows that it is a much better approximation to the numerically calculated front velocity than that given by the leading order theory.

4. $O(\epsilon)$ construction of pulses

How do we correct the pulse construction in Section 2 using our improved theory of wave fronts?

- The region of smooth variation in front of the pulse is as described in Section 2 with the corrections given by Eqs. (28) and (29). In particular, u_n and v_n tend to 0 after a transient stage.

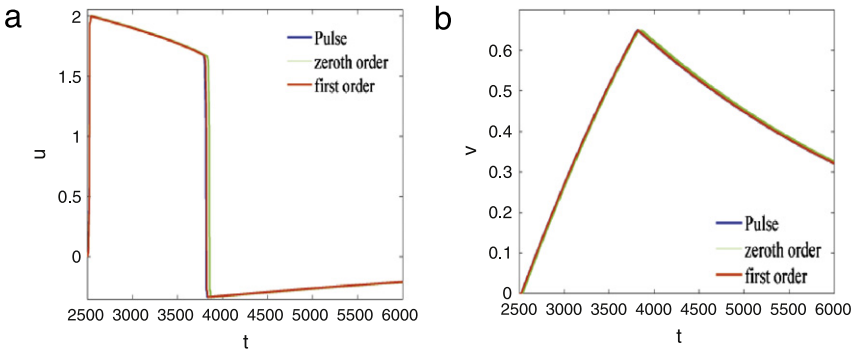

Fig. 6. Comparison of the corrected asymptotic theory with the numerical solution for (a) $u(x, t)$, (b) $v(x, t)$. Here $\epsilon = 0.0003$, $d = 0.1$, $a = B = 0.5$.

- To construct the leading and trailing wave fronts of the pulse, we have to use Eq. (24) instead of Eq. (8), together with Eq. (23) and boundary conditions (26) for the leading DF, and Eq. (24) with Eq. (32) and boundary conditions (33) for the trailing IF. Assume the pulse moves from left to right. The leading wave front is a DF moving with speed $c_-(v)/\epsilon$ with $c_-(v) = c(a, B, v, \epsilon)$, $v = 0$, given by Eqs. (24), (23) and boundary conditions (26). While $v(t)$ is the value at the initial potential u on the first branch of $g(u)$, $v'(t) \neq v(t)$ is the recovery variable at the final point of the DF which is on the third branch of $g(u)$. The time it takes for a point to move from $(u^{(1)}(v), v)$ to $(u^{(3)}(v'), v')$ is of order ϵ and we can ignore it when constructing the pulse. Eventually, $v = 0$, $v' > 0$.
- In the region between leading and trailing fronts, $u_n = u^{(3)}(v_n)$. On its far right, $v_n = v'$, where the DF ends. As we move towards the left, v_n increases until it reaches a certain value $\tilde{V}'(t)$ corresponding to that in the trailing wave front.
- The trailing wave front is an IF moving with speed $c_+(V)/\epsilon$, with $c_+(V) = c(a, B, V, \epsilon)$ given by Eqs. (24), (32) and boundary conditions (33). The recovery variables at the initial and final points of the IF are $\tilde{V}'$ and $\tilde{V}''$, respectively. Again, the time it takes for a point to move from the third to the first branch of the nullcline $v = g(u)$ (on the IF) is of order ϵ.
- The pulse tail is as described in Section 2 with the corrections given by Eqs. (28) and (29), except that its first point has a recovery variable $\tilde{V}''$ instead of V.

Eqs. (10)–(12) become

$$\tau = \int_{v'(t-\tau)}^{V(t)} \frac{dp}{u^{(3)}(p) - Bp}, \tag{35}$$

$$l = \frac{1}{\epsilon} \int_{t-\tau}^{t} c_-(v(t))\, dt. \tag{36}$$

$$\frac{dl}{dt} = \frac{c_-(v'(t)) - c_+(V(t))}{\epsilon}. \tag{37}$$

After the transient period, these equations become

$$\tau = \int_{v'}^{\tilde{V}'} \frac{dv}{u^{(3)}(v) - Bv}, \tag{38}$$

$$l = \frac{c_-(0)\tau}{\epsilon} = \frac{c_-(0)}{\epsilon} \int_{v'}^{\tilde{V}'} \frac{dv}{u^{(3)}(v) - Bv}, \tag{39}$$

$$\frac{dl}{dt} = \frac{c_-(v') - c_+(V)}{\epsilon}. \tag{40}$$

Here v' is fixed, Eq. (39) yields V as a function of l, and then Eq. (40) becomes an autonomous differential equation for $l(t)$. Its stable fixed point l^* and the corresponding time τ^* depend on ϵ because v' and $\tilde{V}'$ do. Except for this, the rest of the considerations made in Section 2 apply.

5. Comparison with the results of direct numerical simulation

We have reconstructed the pulse profile in both the excitatory and the recovery variables using the zeroth and first order approximations for different values of ϵ. The results are presented in Figs. 6 and 7.

For the parameter values in Fig. 1, $d = 0.1$, $a = B = 0.5$ and $\epsilon_c \approx 0.007$. In Fig. 6, we show the pulse profiles for $\epsilon = 0.0003$ ($-\ln\epsilon = 8.11$) and observe that the reconstruction of the pulse is already quite good for the leading zeroth order theory. The first order theory provides an even better approximation. Fig. 3 shows that the numerically calculated and

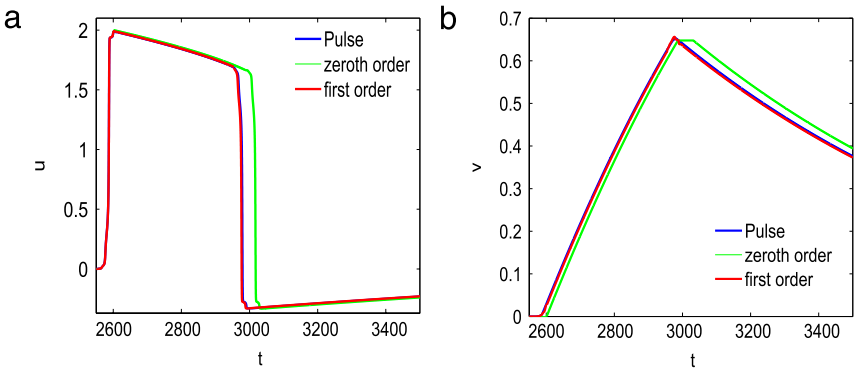

Fig. 7. Comparison of the corrected asymptotic theory with the numerical solution for (a) $u(x, t)$, (b) $v(x, t)$. Here $\epsilon = 0.001$, $d = 0.1$, $a = B = 0.5$.

approximated pulse velocities are quite close for this value of ϵ, so having a good reconstruction of the pulse for this value comes as no surprise.

The value $\epsilon = 0.001$ ($-\ln\epsilon = 6.91$) used in the reconstructions depicted in Fig. 7 is closer to $\epsilon_c \approx 0.007$. Fig. 3 shows that the numerically calculated and approximated pulse velocities are not very close for this value of ϵ, and that the first order theory gives a better pulse velocity than the zeroth order theory (horizontal line in Fig. 3). Then, we can appreciate some differences between the zeroth order and first order reconstructions of the pulse in Fig. 7(a) and (b). The first order theory yields a better reconstruction and the differences with the numerically calculated pulse can be explained by the error in the calculation of the pulse velocity as observed in Fig. 3.

6. Conclusion

Spatially discrete excitable systems exhibit pulse solutions that can be constructed using matched asymptotic expansions which exploit the large separation of time scales in their dynamics (as measured by a small dimensionless parameter ϵ). The pulse profile typically consists of slowly varying regions of the excitatory variable separated by sharp wave fronts. In the FHN system, the velocity of a pulse is decided by the interaction between its leading and trailing fronts. We have shown how to find a better approximation to the wave fronts comprising the FHN pulse. Our approximation provides a pulse velocity that depends on ϵ and compares much better with the velocity obtained from numerical solutions. As a result, the reconstruction of the FHN pulse shape using the improved wave fronts also compares much better with the numerically obtained pulse.

Acknowledgements

This work has been financed by the Spanish Ministerio de Economia y Competitividad grants FIS2008-04921-C02-01 and FIS2011-28838-C02-01 and by the Autonomous Region of Madrid grant P2009/ENE-1597 (HYSYCOMB).

References

[1] J. Frenkel, T. Kontorova, On the theory of plastic deformation and twinning, J. Phys. (Moscow) 1 (1939) 137–149.
[2] A. Carpio, L.L. Bonilla, Edge dislocations in crystal structures considered as traveling waves of discrete models, Phys. Rev. Lett. 90 (2003) 135502 (4 pp).
[3] J.W. Cahn, Theory of crystal growth and interface motion in crystalline materials, Acta Metall. 8 (1960) 554–562.
[4] L.L. Bonilla, Theory of nonlinear charge transport, wave propagation and self-oscillations in semiconductor superlattices, J. Phys.: Condens. Matter 14 (2002) R341–R381.
[5] A. Carpio, L.L. Bonilla, G. Dell'Acqua, Motion of wave fronts in semiconductor superlattices, Phys. Rev. E 64 (2001) 036204 (9 pp).
[6] L.L. Bonilla, S.W. Teitsworth, Nonlinear Wave Methods for Charge Transport, Wiley, Weinheim, 2010.
[7] J.I. Arana, L.L. Bonilla, H.T. Grahn, Wave fronts, pulses and wave trains in photoexcited superlattices behaving as excitable or oscillatory media, J. Phys. A 44 (2011) 395003 (19 pp).
[8] G. Grüner, The dynamics of charge-density waves, Rev. Mod. 60 (1988) 1129–1181.
[9] A.C. Scott, The electrophysics of a nerve fiber, Rev. Mod. 47 (1975) 487–533.
[10] A.R.A. Anderson, B.D. Sleeman, Wave front propagation and its failure in coupled systems of discrete bistable cells modelled by FitzHugh–Nagumo dynamics, Internat. J. Bifur. Chaos 5 (1995) 63–74.
[11] J.P. Keener, J. Sneyd, Mathematical Physiology, Springer, New York, 1998, (Chapter 9).
[12] B. Zinner, Existence of traveling wavefront solutions for the discrete Nagumo equation, J. Differential Equations 96 (1992) 1–27.
[13] D. Hankerson, B. Zinner, Wave fronts for a cooperative tridiagonal system of differential equations, J. Dynam. Differential Equations 5 (1993) 359–373.
[14] A.-M. Filip, S. Venakides, Existence and modulation of traveling waves in particle chains, Comm. Pure Appl. Math. 52 (1999) 693–735.
[15] P.C. Fife, Mathematical Aspects of Reacting and Diffusing Systems, in: Lecture Notes in Biomathematics, vol. 28, Springer-Verlag, Berlin, 1979.
[16] A. Carpio, L.L. Bonilla, Pulse propagation in discrete systems of coupled excitable cells, SIAM J. Appl. Math. 63 (2003) 619–635.
[17] J.P. Keener, Propagation and its failure in coupled systems of discrete excitable cells, SIAM J. Appl. Math. 47 (1987) 556–572.
[18] A. Carpio, L.L. Bonilla, Depinning transitions in discrete reaction–diffusion equations, SIAM J. Appl. Math. 63 (2003) 1056–1082.
[19] H.J. Hupkes, D. Pelinovsky, B. Sandstede, Propagation failure in the discrete Nagumo equation, Proc. Amer. Math. Soc. 139 (2011) 3537–3551.
[20] J.P. Keener, J.J. Tyson, Singular perturbation theory of traveling waves in excitable media (a review), Physica D 32 (1988) 327–361.

[21] A. Carpio, Wave trains, self-oscillations and synchronization in discrete media, Physica D 207 (2005) 117–136.
[22] H.J. Hupkes, D. Pelinovsky, B. Sandstede, Travelling pulses for the discrete FitzHugh–Nagumo system, SIAM J. Appl. Dyn. Syst. 9 (2010) 827–882.
[23] H.J. Hupkes, D. Pelinovsky, B. Sandstede, Stability of pulse solutions for the discrete FitzHugh–Nagumo system, Trans. Amer. Math. Soc. (2012) (in press).
[24] A. Carpio, I. Peral, Propagation failure along myelinated nerves, J. Nonlinear Sci. 21 (2011) 499–520.
[25] N. Kurata, H. Kitahata, H. Mahara, A. Nomura, H. Miike, T. Sakurai, Stationary pattern formation in a discrete excitable system with strong inhibitory coupling, Phys. Rev. E 79 (2009) 056203 (5 pp).
[26] L.D. Weise, M.P. Nash, A.V. Panfilov, A discrete model to study reaction–diffusion-mechanics systems, PLoS One 6 (2011) e21934 (13 pp).
[27] L.D. Weise, A.V. Panfilov, New mechanism of spiral wave initiation in a reaction–diffusion-mechanics system, PLoS One 6 (2011) e27264 (9 pp).
[28] G. Lin, W.-T. Li, Traveling waves in delayed lattice dynamical systems with competition interactions, Nonlinear Anal. RWA 11 (2010) 3666–3679.
[29] G. Lv, M. Wang, Nonlinear stability of traveling wave fronts for delayed reaction–diffusion systems, Nonlinear Anal. RWA 13 (2012) 1854–1865.
[30] O. Vallès-Codina, R. Möbius, S. Rüdiger, L. Schimansky-Geier, Traveling echo waves in an array of excitable elements with time-delayed coupling, Phys. Rev. E 83 (2011) 036209 (9 pp).